

This work was supported by a Grant-in-Aid for Scientific Research from the Ministry of Education, Science and Culture, Japan.

References

- BONDI, A. (1964). *J. Phys. Chem.* **68**, 441–451.
International Tables for X-ray Crystallography (1974). Vol. IV, pp. 71–151. Birmingham: Kynoch Press.
 KURIHARA, T., OHASHI, Y. & SASADA, Y. (1982). *Acta Cryst.* **B38**, 2484–2486.
 MAIN, P., HULL, S. E., LESSINGER, L., GERMAIN, G., DECLERCQ, J. P. & WOLFSON, M. M. (1978). *MULTAN 78. A System of Computer Programs for the Automatic Solution of Crystal Structures from X-ray Diffraction Data*. Univs. of York, England, and Louvain, Belgium.
 OHASHI, Y. (1975). Unpublished. Original *HBL*S program by T. ASHIDA.
 OHASHI, Y., KURIHARA, T., SASADA, Y. & OHGO, Y. (1981). *Acta Cryst.* **A37**, C-88.
 OHASHI, Y. & SASADA, Y. (1977). *Nature (London)*, **267**, 142–144.
 OHASHI, Y., SASADA, Y. & OHGO, Y. (1978a). *Chem. Lett.* pp. 457–460.
 OHASHI, Y., SASADA, Y. & OHGO, Y. (1978b). *Chem. Lett.* pp. 743–746.
 OHASHI, Y., YANAGI, K., KURIHARA, T., SASADA, Y. & OHGO, Y. (1981). *J. Am. Chem. Soc.* **103**, 5805–5812.
 OHASHI, Y., YANAGI, K., KURIHARA, T., SASADA, Y. & OHGO, Y. (1982). *J. Am. Chem. Soc.* **104**, 6353–6359.
 SHELDRIK, G. M. (1976). *SHELX 76*. Program for crystal structure determination. Univ. of Cambridge, England.
 UCHIDA, A., OHASHI, Y., SASADA, Y. & OHGO, Y. (1982). In preparation.

Acta Cryst. (1983). **B39**, 61–75

Experimental *versus* Theoretical Charge Densities: a Hydrogen-Bonded Derivative of Bicyclobutane at 85 K

BY M. EISENSTEIN AND F. L. HIRSHFELD

Department of Structural Chemistry, Weizmann Institute of Science, Rehovot, Israel

(Received 10 September 1981; accepted 5 May 1982)

Abstract

The charge deformation density in 1,3-diethylbicyclobutane-*exo,exo*-2,4-dicarboxylic acid has been mapped by least-squares refinement against low-temperature X-ray data extending to $2 \sin \theta/\lambda = 2.73 \text{ \AA}^{-1}$. Results agree semi-quantitatively with *ab initio* calculations on bicyclobutane, ethane, and formic acid cyclic dimer. Experimental and theoretical deformation densities show similar bond bending in the bicyclobutane nucleus, similar net charges and moments of corresponding atomic fragments, and a similar charge distribution in the hydrogen-bonded carboxylic acid. Wide variability in C–C bond lengths and dihedral angle in several substituted bicyclobutanes implies great flexibility for this strained system. [Crystal data at 85 K: $C_{10}H_{14}O_4$, $P2_1/c$, $a = 7.627(2)$, $b = 9.306(2)$, $c = 16.928(6) \text{ \AA}$, $\beta = 121.53(3)^\circ$; $R = 0.0917$, $R_w = 0.0650$ for 9103 reflections.]

reliability of such maps is by comparison with charge densities derived from *ab initio* calculations. Such a comparison provided strong support for the experimental static deformation density of diformohydrazide (Eisenstein, 1979) derived from the low-temperature X-ray data of Hope & Ottersen (1978). Further comparisons of the same sort are needed to establish the conditions leading, on the one hand, to reliable experimental charge densities and, on the other, to accurate theoretical maps. The present study applies such a test to the experimental deformation density of 1,3-diethylbicyclobutane-*exo,exo*-2,4-dicarboxylic acid (DBDA). It thus combines an investigation of the charge distribution in a particular strained molecule of great chemical interest with a contribution to the methodology of experimental and theoretical charge density studies.

The DBDA molecule comprises a bicyclobutane nucleus substituted at all four C atoms. The bridge atoms carry ethyl substituents while the other two ring atoms have carboxylic acid substituents in the *exo* positions. These carboxyl groups form cyclic hydrogen-bonded links with neighboring molecules related by a crystallographic glide plane. The several portions of the molecule may be compared with the three model compounds bicyclobutane, ethane, and formic acid

Experimental charge density studies by means of accurate X-ray diffraction measurements have been found capable, in favorable circumstances, of yielding detailed deformation density maps of at least semi-quantitative significance. One way of testing the

cyclic dimer, all small enough to permit moderately sophisticated *ab initio* calculations.

Experimental

Crystals suitable for intensity measurement were grown during several days by vapor-phase diffusion of *n*-heptane into a water solution of the compound. With increasing concentration of *n*-heptane the solubility of the dicarboxylic acid decreased and crystals gradually precipitated. The single crystal selected for diffractometry had a roughly spherical shape with largest diameter 0.3 mm.

The X-ray intensities were measured at 85 ± 1 K on a four-circle CAD-4 diffractometer bearing a gas-flow cooling device supplied by Enraf-Nonius and modified by Professor H. Hope. Long-term temperature fluctuations, monitored by a thermocouple placed inside the nozzle upstream of the crystal, were less than ± 0.5 K. Graphite-monochromated Mo $K\alpha$ radiation was used and the intensities were recorded with an $\omega/2\theta$ scan sampled at 96 points. The scan range was 1.5 times the α_1 - α_2 separation, plus an additional 0.6° in θ at each end. The scan rate was chosen so as to allot, in most cases, a maximum counting time of 120 or 180 s for the full scan. A rapid prescan of each reflection permitted some saving of time in two opposite circumstances. Strong reflections were scanned at a faster rate selected to achieve a relative precision of 1% in the net intensity I_{net} , provisionally defined as the sum of the central 64 counts minus twice the sum of the outer 32 counts. Very weak reflections, on the other hand, were not rescanned at all if it appeared that the preselected maximum time would not yield a relative precision $\sigma(I_{\text{net}})/I_{\text{net}}$ appreciably under 0.5. Three moderately strong reflections were monitored at intervals of about 2 h. These showed a long-term intensity drift approaching 5%, which was corrected by a smoothly interpolated drift curve.

Most reflections were measured in the standard bisecting geometry, with the imaginary χ circle of the diffractometer bisecting the angle between the incident and reflected X-ray beams. However, the crystal orientation was checked for the possibility of multiple reflections (Coppens, 1968). If the standard geometry for reflection \mathbf{H} ($=hkl$) placed a second reciprocal-lattice point \mathbf{H}' too near the Ewald sphere, where either \mathbf{H}' or $\mathbf{H} - \mathbf{H}'$ (or their symmetry equivalents) appeared in a list of the few dozen strongest reflections, the crystal was rotated about the Bragg vector \mathbf{H} to a safe orientation.

Data collection proceeded in two stages. In the first stage all 2995 independent reflections at $\theta < 30^\circ$ were scanned, plus several hundred equivalent reflections in a second quadrant to allow a check on the internal consistency of the measured intensities. For most of

these low-angle reflections a maximum counting time of 120 s was allotted to each scan. For the second stage, calculated structure amplitudes based on a preliminary structure refinement were used to predict the approximate intensities of all reflections in the range $30^\circ < \theta < 76^\circ$. The prediction identified those reflections whose net intensities were expected to be measurable to a relative precision under 0.5. These numbered 6108 independent reflections and they alone were scanned, together with a sizable proportion of symmetry-equivalent reflections, for a maximum counting time of 180 s. Despite the preselection, many of the high-order reflections were close to background level and several hundred yielded negative net intensities. For the weakest reflections only the fast prescan was performed and these data have correspondingly small statistical weight. In all, 11478 reflections were recorded, of which 9103 were independent, to a maximum reciprocal radius $S = 2 \sin \theta / \lambda = 2.73 \text{ \AA}^{-1}$.

To improve the statistical accuracy, especially of the weak reflections, the actual background correction was deduced from a smooth background function fitted to the outer portions of the reflection scans. For this purpose the sum of the ten outermost counts of each reflection profile, five at each end of the scan, was taken to represent the background intensity at the appropriate values of the orientation angles θ , χ , and φ . Strong reflections whose tails, extending into these outer regions, might bias the background estimates were discarded from the sample. The remaining 10444 background values b_i , scaled to a common scan rate and appropriately weighted, were fitted by a smooth function having the form

$$B(\theta, \chi, \varphi) = B_o B_\theta(\theta) B_\chi(\chi) B_\varphi(\varphi).$$

The constant B_o is an overall scale factor that was extracted from the several functions B_θ , B_χ , and B_φ . The θ -dependent function B_θ contains most of the observed variation in B and was represented by a tenth-degree polynomial in θ . Its form is shown in Fig. 1(a). The variation in χ and φ was far more moderate and was adequately represented by a fourth-degree polynomial in χ and by a third-degree polynomial in $\cos(\varphi - \varphi_o)$, with the angle φ_o constituting a fourth adjustable parameter for the function B_φ (Fig. 1b,c). The overall fit of the function B to the measured values b_i may be gauged by the goodness of fit

$$G = \left[\sum_i w_i (b_i - B)^2 / (10444 - p) \right]^{1/2} = 1.12,$$

where w_i is the statistical weight of the quantity b_i , estimated by Poisson counting statistics, and $p = 1 + 10 + 4 + 4 = 19$ is the number of independent parameters in the fitted function $B(\theta, \chi, \varphi)$. The quality of the match in different ranges of θ , χ , and φ provided an estimate of the standard deviation $\sigma(B)$ as a

motion of each of the substituent groups was converted into an equivalent set of T, L, and S tensors, referred to the common molecular origin, and these were added to the corresponding tensors of the central segment. In this way five sets of rigid-body tensors were derived, each specifying the vibrational motion of a skeletal segment to which the corresponding H atoms could be attached. These tensors were repeatedly adjusted in the same manner as the deformation refinement proceeded towards convergence.

Once the five sets of rigid-body tensors had been derived, the constraints on the heavy-atom vibrations were removed and their harmonic vibration parameters were refined independently. Only the H vibration parameters were derived from the rigid-body tensors of the appropriate molecular segments, to which were added internal C–H and O–H stretching and bending vibrations estimated from the infrared frequencies of methanol (Margottin-Maclou, 1960). Thus all C–H bonds were assigned mean-square stretching and bending amplitudes of 0.0057 and 0.0115 Å², respectively, while the O–H bonds were assigned corresponding mean-square amplitudes of 0.0045 and 0.0120 Å². The torsional motions of the methyl and hydroxyl H atoms about the respective C–C or C–O bond axes were refined independently. The four torsional amplitudes, for the two methyl and two hydroxyl groups, were the only adjustable vibration parameters employed for the H atoms.

The charge deformation density was modeled by a rather flexible atomic multipole expansion (Hirshfeld, 1977a), but this was applied conservatively, with the number of refined parameters restricted in various ways. First, identical multipole coefficients were assigned to pairs of atoms related by the non-crystallographic molecular twofold axis. Further, the ten H atoms of the methylene and methyl groups were all made equivalent in their deformations. Of the atomic multipole functions.

$$\rho_{a,n,k} = N_n r^n \exp(-\alpha_a r_a) \cos^n \theta_k \quad (1)$$

with $n \leq 4$, those with $n = 0$ (cusp functions) were omitted for C and O and those with $n = 4$ were, as usual, omitted for H. Each C and O atom was constrained to local mirror symmetry (with 21 independent coefficients), while the methyl C atoms were assigned symmetry $3m$ (10 coefficients). The H atoms, which were contracted isotropically by a linear factor of 1.2 before addition of the multipole functions (Harel & Hirshfeld, 1975), were made axially symmetric (six coefficients) about the respective C–H or O–H bond axes. Also, the exponential factor α_a was made equal for all three types of H atom (ring, ethyl, and hydroxyl). Finally, the net molecular charge was constrained to zero. This model had eight exponential factors α_a (one for H, five for C, two for O) and 153

independent expansion coefficients (18 for H, 94 for C, 42 for O, minus 1 neutrality constraint).

As the deformation refinement proceeded, the two O–H bond lengths tended towards unreasonably short values. They were accordingly fixed at an assumed (uncorrected) value of 0.975 Å.

In all, 333 independent parameters were ultimately refined. These comprised the scale factor k , the extinction coefficient c , 82 positional coordinates for the 28 atoms (allowing for two constrained O–H distances), 88 vibration parameters (84 for 14 heavy atoms plus 4 for hydrogen), and 161 deformation parameters. The rigid-body tensor components are not counted as parameters because their definition depends on vibrational constraints that were discarded in the final model.

At high Bragg angles all reflection profiles are broadened by spectral dispersion beyond the limits of any feasible scan range (Denne, 1977). One symptom of this effect was noted during the derivation of the background function B (see above). This was a linear dependence of the apparent background on the intensities of the associated reflections, due to the intrusion of the Bragg reflections into the 'background' regions. But contrary to the expected behavior, the slope of this dependence was found to reach a maximum near $\theta = 70^\circ$ and to decrease at higher values of θ . A similar anomaly became apparent in the θ dependence of average values of F_o/kF_c . The weighted mean square of this ratio, evaluated as

$$\langle F_o^2/k^2 F_c^2 \rangle_w = \sum w F_o^2 F_c^2 / \sum w k^2 F_c^4,$$

fluctuated moderately about 1.028 in the range $\theta < 35^\circ$ and then fell steeply to a minimum of 0.92 near $\theta = 60^\circ$ before rising again to well above 1.1 for the highest-angle reflections. Since no plausible truncation model could account for this behavior, no correction for the effect was applied to the measured intensities. But the recognition that our high-angle data apparently suffer from some unexplained systematic error was an important factor in the decision not to refine cusp coefficients on the heavy atoms. Inclusion of such functions might have reduced slightly the high-angle discrepancy between F_o and F_c but, in the absence of a valid truncation correction, the apparent improvement would have been largely artificial. The uncorrected truncation error and the consequent limitation on the deformation model combine to cast severe doubt on the absolute magnitudes of the refined atomic vibration parameters.

The refinement converged to the somewhat disappointing discrepancy indices $R = \sum |F_o - k|F_c| / \sum |F_o| = 0.0917$,* $R_w = [\sum w(F_o^2 - k^2 F_c^2)^2 / \sum w F_o^4]^{1/2} = 0.0650$, $G = [\sum w(F_o^2 - k^2 F_c^2)^2 / (N - p)]^{1/2} = 1.238$.

* In the evaluation of R , 550 reflections with negative values of F_o^2 were included with F_o defined as $F_o = -|F_o^2|^{1/2}$. Exclusion of these reflections yields $R = 0.0721$.

The large values of R and R_w may be attributed both to the systematic error in the high-angle intensities, which also contributes to the elevated value of G , and to the inclusion of many imprecisely measured weak reflections.

Final atomic coordinates and vibration parameters are listed in Table 1.*

* A list of structure factors has been deposited with the British Library Lending Division as Supplementary Publication No. SUP 38003 (24 pp.). Copies may be obtained through The Executive Secretary, International Union of Crystallography, 5 Abbey Square, Chester CH1 2HU, England.

Several routine tests were applied to the results of the deformation refinement. One was to examine the mean-square goodness of fit, as measured by the subset averages $\langle w(F_o^2 - k^2 F_c^2)^2 \rangle$, as a function both of F^2 and of S . These averages were reassuringly constant, varying between 1.0 and 1.4 in different ranges of F_o^2 , except for $F_o^2 < 0$, and between 1.0 and 1.7 in different ranges of S . Secondly, the residual difference density $\Delta\rho(\mathbf{r})$, evaluated by Fourier transformation of the discrepancies $\Delta F = F_o/k - F_c$, showed largely random noise with an evident predominance of moderately high-frequency Fourier components. Very few features

Table 1. *Positional parameters and thermal parameters*

(a) Fractional atomic coordinates ($\times 10^5$ for heavy atoms, $\times 10^4$ for H); estimated standard deviations in the last digit are in parentheses

	<i>x</i>	<i>y</i>	<i>z</i>		<i>x</i>	<i>y</i>	<i>z</i>
C(1)	34258 (15)	17831 (10)	66064 (4)	H(2)	1873 (18)	-125 (60)	6864 (8)
C(2)	21428 (7)	10800 (9)	69457 (5)	H(4)	1931 (17)	-49 (60)	5561 (8)
C(3)	12198 (14)	20234 (11)	60873 (4)	H(5a)	5330 (15)	3374 (34)	6575 (23)
C(4)	21614 (7)	11586 (9)	56387 (5)	H(5b)	5287 (15)	3306 (31)	7601 (24)
C(5)	53590 (13)	26496 (9)	70803 (4)	H(6a)	8670 (64)	2401 (36)	7872 (18)
C(6)	72946 (16)	17295 (10)	75082 (6)	H(6b)	7299 (17)	1000 (35)	8015 (24)
C(7)	23426 (6)	16852 (12)	77974 (6)	H(6c)	7350 (16)	1065 (32)	7003 (27)
C(8)	-2281 (13)	32771 (9)	57635 (5)	H(8a)	332 (29)	4040 (36)	5468 (16)
C(9)	-24541 (18)	28780 (8)	50666 (7)	H(8b)	-91 (17)	3765 (25)	6375 (28)
C(10)	23480 (6)	18346 (12)	48932 (6)	H(9a)	-3435 (47)	3807 (47)	4878 (10)
O(1)	25542 (6)	29776 (13)	79758 (6)	H(9b)	-2983 (27)	2056 (40)	5335 (17)
O(2)	22906 (6)	7044 (11)	83434 (7)	H(9c)	-2584 (18)	2402 (23)	4443 (29)
O(3)	24955 (5)	31368 (13)	48180 (6)	H(O2)*	2403	1145	8891
O(4)	23277 (6)	8800 (11)	43164 (7)	H(O4)*	2502	1353	3848

(b) Atomic vibration parameters ($\text{\AA}^2 \times 10^{-3}$); the temperature factor has the form $\exp(-2\pi^2 \sum_i \sum_j h_i h_j a^i a^j U^{ij})$

	U^{11}	U^{22}	U^{33}	U^{12}	U^{23}	U^{13}
C(1)	979 (21)	1159 (21)	978 (16)	-62 (19)	-38 (15)	482 (14)
C(2)	1274 (19)	1116 (19)	1043 (16)	-29 (14)	41 (14)	655 (14)
C(3)	998 (21)	1162 (21)	989 (17)	38 (19)	42 (15)	490 (14)
C(4)	1320 (19)	1161 (20)	1028 (16)	-114 (14)	-100 (15)	664 (14)
C(5)	1131 (20)	1473 (21)	1488 (19)	-217 (18)	-235 (15)	642 (15)
C(6)	1161 (21)	2672 (29)	4303 (36)	210 (23)	-820 (27)	517 (21)
C(7)	1320 (21)	1148 (22)	1050 (17)	29 (14)	64 (17)	696 (14)
C(8)	1340 (20)	1292 (20)	1374 (17)	197 (18)	79 (16)	588 (16)
C(9)	1335 (26)	2317 (28)	3546 (31)	398 (20)	-402 (24)	-78 (23)
C(10)	1414 (21)	1256 (23)	1042 (17)	-109 (14)	-71 (17)	694 (15)
O(1)	2425 (27)	1154 (21)	1350 (16)	-172 (12)	-81 (16)	1236 (16)
O(2)	2074 (26)	1270 (20)	1383 (17)	40 (12)	215 (17)	1149 (15)
O(3)	2460 (27)	1191 (22)	1432 (16)	-237 (12)	-103 (15)	1285 (18)
O(4)	2850 (29)	1321 (20)	1461 (17)	-173 (13)	-233 (16)	1446 (19)
H(2)	2817	1630	2411	-161	-75	1518
H(4)	2658	1694	2335	-233	-173	1409
H(5a)	3053	3499	2578	-1136	299	1255
H(5b)	2859	3772	3149	-1072	-1638	1908
H(6a)	1845	4432	7375	-583	-1023	948
H(6b)	3406	5596	7698	690	3382	607
H(6c)	3356	6127	9888	347	-3770	2945
H(8a)	3524	2621	4185	747	1282	2568
H(8b)	3729	3172	2180	1236	29	1443
H(9a)	2577	3919	5980	1307	-180	493
H(9b)	2509	4457	10833	-385	1209	2258
H(9c)	4489	6625	4051	1713	-2415	-876
H(O2)	4227	2591	2209	-28	-264	2107
H(O4)	4079	2734	2413	-315	135	2241

* Hydroxyl H atoms, refined in local polar coordinate systems, have independent coordinates given by:

	r_{O-H} (assumed)	φ_{C-O-H}	$\theta_{O=C-O-H}$
H(O2)	0.975 Å	110.8 (8)°	1.5 (3)°
H(O4)	0.975	110.2 (8)	2.3 (4)

Table 2. Mean-square vibration amplitudes of bonded atoms *A* and *B* in the direction of bond *A*—*B* ($\text{\AA}^2 \times 10^{-5}$)

<i>A</i>	<i>B</i>	$z_{A,B}^2$	$z_{B,A}^2$	<i>A</i>	<i>B</i>	$z_{A,B}^2$	$z_{B,A}^2$
C(1)	C(3)	1002	990	C(3)	C(8)	1062	1121
C(1)	C(2)	1037	1048	C(8)	C(9)	1385	1332
C(2)	C(3)	1019	1011	C(4)	C(10)	1028	1037
C(3)	C(4)	1090	1103	C(7)	O(1)	1170	1129
C(4)	C(1)	993	970	C(7)	O(2)	985	918
C(1)	C(5)	974	1033	C(10)	O(3)	1239	1152
C(5)	C(6)	1433	1415	C(10)	O(4)	1081	978
C(2)	C(7)	1038	1017				

$$\Delta z^2 (\text{r.m.s.}) = 49 \text{ (33 for C—C only).}$$

exceeded $\pm 0.5 e \text{\AA}^{-3}$ but the deepest hollows occurred systematically at the positions of the heavy atoms. This is the only clearly non-random pattern in the residual density and is surely related to the systematic discrepancy in the high-angle intensities. Thirdly, the total static density, *i.e.* promolecule plus deformation density, was scanned throughout the asymmetric unit for possible negative values and none at all were found. Finally, the refined vibration parameters were tested against the rigid-bond postulate (Hirshfeld, 1976). The r.m.s. difference $z_{A,B}^2 - z_{B,A}^2$ (Table 2) was found to be under 0.0005\AA^2 , compared with estimated standard deviations $\sigma(U^{ii})$ for the several C and O atoms ranging between 0.0002 and 0.0003\AA^2 (Table 1*b*). Moreover, even the largest of these differences are barely significant, are limited to the C—O bonds, and are systematic, implying marginally smaller vibration amplitudes, along the bonds, for the heavier O atoms. The principal conclusion from this test is that, despite doubts about the high-angle intensities and the severely constrained deformation model, the deconvolution of the vibrational motion appears to have been strikingly successful. This conclusion does not rule out the suspicion of a systematic error, possibly anisotropic, affecting the vibration parameters of all atoms equally.

Molecular dimensions

The experimental bond lengths (Table 3) were corrected for vibrational shortening in accordance with the same segmented model that served for the derivation of the H vibration parameters. C—C bond lengths within the bicyclobutane nucleus and those radiating from it were corrected for rigid-body libration only. The ethyl C—C bonds and the four C—O bonds were corrected additively for molecular libration and for torsional motion about the respective exocyclic C—C bonds. The C—H and O—H distances were adjusted similarly and, in addition, were corrected for bending vibrations in two dimensions. Except for the methyl groups, the total corrections to the C—H and O—H bond lengths are

nearly as large as would be deduced from the riding model (Busing & Levy, 1964).

The dimensions of the bicyclobutane nucleus, where the bridge bond C(1)—C(3) is shorter by almost 0.07\AA than the lateral C—C bonds (Fig. 2), contrast sharply with those found in bicyclobutane itself, for which microwave (Cox, Harmony, Nelson & Wiberg, 1969, 1970), electron diffraction (Bastiansen, 1970, unpublished; cited in Meiboom & Snyder, 1971), and NMR studies (Meiboom & Snyder, 1971) agree in assigning equal lengths to all five C—C bonds, about 1.497 to 1.507\AA . The present value of 1.452\AA for the bridge bond is somewhat suspect because of an anomalously large gradient in the deformation density at the bridgehead atoms (see below); this could mean that these atoms have refined to severely incorrect positions. The observed gradient arises primarily from the dipolar ($n = 1$) deformation functions [see eq. (1)] on the two atomic centers, and the relevant least-squares covariances imply that setting the coefficients of these dipolar functions to zero would cause the C(1)—C(3) distance to increase by 0.0063\AA . This would still leave a highly significant difference of 0.061\AA between the two kinds of C—C bond in the bicyclobutane nucleus.

Table 4 presents a compilation of pertinent dimensions in several bicyclobutane derivatives, most of them

Table 3. Bond lengths (\AA), corrected for molecular libration, torsion, and bending

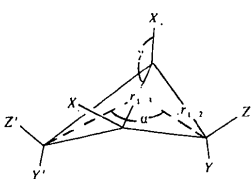
	Refined	Correction ($\text{\AA} \times 10^{-3}$)*			Corrected
		Libration	Torsion†	Bending‡	
C(1)—C(2)	1.5182 (10)	111			1.5193
C(2)—C(3)	1.5190 (10)	128			1.5203
C(3)—C(4)	1.5206 (11)	80			1.5214
C(4)—C(1)	1.5156 (10)	99			1.5166
C(1)—C(3)	1.4504 (18)	148			1.4519
C(1)—C(5)	1.4928 (13)	142			1.4942
C(5)—C(6)	1.5222 (15)	149	1283		1.5365
C(2)—C(7)	1.4800 (13)	66			1.4807
C(7)—O(1)	1.2302 (15)	98	16		1.2314
C(7)—O(2)	1.3146 (14)	104	21		1.3159
C(3)—C(8)	1.4991 (13)	140			1.5005
C(8)—C(9)	1.5210 (15)	151	1298		1.5355
C(4)—C(10)	1.4827 (13)	94			1.4836
C(10)—O(3)	1.2301 (15)	109	275		1.2340
C(10)—O(4)	1.3145 (14)	68	368		1.3188
C(2)—H(2)	1.136 (57)	9		102	1.147
C(4)—H(4)	1.135 (57)	9		102	1.146
C(5)—H(5a)	1.080 (49)	9	99	104	1.102
C(5)—H(5b)	1.098 (49)	6	99	104	1.119
C(6)—H(6a)	1.093 (52)	10	1	219	1.116
C(6)—H(6b)	1.092 (52)	9	98	218	1.125
C(6)—H(6c)	1.074 (52)	6	97	222	1.106
C(8)—H(8a)	1.077 (50)	9	101	104	1.099
C(8)—H(8b)	1.085 (49)	5	101	104	1.106
C(9)—H(9a)	1.077 (52)	10	1	187	1.096
C(9)—H(9b)	1.070 (53)	9	97	186	1.100
C(9)—H(9c)	1.100 (51)	5	104	181	1.129
O(2)—H(O2)	0.975	4	0	158	0.991
O(4)—H(O4)	0.975	6	0	106	0.986
O(3)—H(O2')	1.674				
O(3)—O(2')	2.6482 (15)				
O(1)—H(O4')	1.623				
O(1)—O(4')	2.5932 (15)				

* $\text{\AA} \times 10^{-3}$ for C—H and O—H.

† About the exocyclic C—C bond.

‡ For methyl C—H this correction is due mainly to torsional vibration of the entire methyl group, inseparable by Bragg experiment from bending of each C—H bond normal to the local C—C—H plane.

Table 4. Dimensions (Å and deg) of bicyclobutane derivatives



Compound ^(a)	X	Y, Y'	Z, Z'	α	r_{1-3}	r_{1-2}	$\langle r \rangle^{(b)}$	$\Delta r^{(c)}$	γ	Reference
DPHTCP	Ph	—CH— OC(O)PhBr	H ₂	95.1	1.44	1.53	1.50	-0.09 ₅	138.8	(e)
BVAL	H	—HC=CH—	H ₂	106.0	1.452	1.529	1.503	-0.077	133.7	(f)
MTSHCH	Me	—C—C— TosHNN NNHTos	H ₂	110.7	1.455	1.540	1.512	-0.085	140.0	(g)
DBDA	Et	H ₂	(COOH) ₂	112.8	1.452	1.519 ₄	1.497	-0.067 ₅	138.1	This work
DBPCDD	Anthracene (9,10)bridge	—(CH ₂) ₂ —	H ₂	113	1.54	1.51	1.52	0.03		(h)
FMOPCU	CF ₃	—(CF ₃)C—C(CF ₃)— HCOCH BrHC CHBr	(CF ₃) ₂	113.2	1.39	1.48	1.45	-0.09	137.3	(i)
TMTCHD	Me	—C—C— O O	Me ₂	114	1.48	1.57	1.54	-0.09	138	(j)
NTCHPE	H	Naphthalene (1,8)bridge	H ₂	120.3	1.47	1.49	1.48 ₅	-0.02 ₆	128	(k)
XZTCDD	Me	—C—N—C— O O N C—COOMe C—COOMe	Me ₂	120.5	1.473	1.519	1.504	-0.046	137.7	(l)
HEPANT	Anthracene (9,10)bridge	—(CH ₂) ₃ —	H ₂	120.7	1.549	1.516	1.527	0.033	(110.2) ^(d)	(m)
MXCPBU	Ph	COOMe, H	H, COOMe	120.7	1.51 ₆	1.52 ₂	1.52	-0.00 ₆	139.6	(n)
BCB	H	H ₂	H ₂	121.7	1.497	1.498	1.498	-0.001	128.4	(o)
THCUNT	H	—SPh—	H ₂	122	1.483	1.487	1.486	-0.004	~130	(p)
PHTCHP	H	Phenanthrene (1,10)bridge	H ₂	122.4	1.47 ₁	1.48 ₉	1.48 ₃	-0.01 ₈		(q)
EMYEST	H	—HCPh(OMe)— (CH ₂) ₂	—HC—(CH ₂) ₂ , H MeC—C—O O—(CH ₂) ₂	122.5	1.512	1.497	1.502	0.015	121	(r)
DCYBUT	CN	H ₂	H ₂	126.4	1.503	1.482 ₅	1.489	0.020 ₅	124.6	(s)
MTMBCO	SMe	Me ₂	Me ₂	128.7	1.514	1.513 ₅	1.514	0.000 ₅	130.9	(t)
MCDPCB	Ph	(COOMe) ₂	H ₂	129.7	1.57 ₄	1.51 ₇	1.53 ₆	0.05 ₇	131.2	(u)

Notes: (a) Six-letter codes are from the Cambridge Data File. (b) $\langle r \rangle = \frac{1}{3}r_{1-3} + \frac{2}{3}r_{1-2}$. (c) $\Delta r = r_{1-3} - r_{1-2}$. (d) γ constrained by anthracene bridge. (e) Gibbons & Trotter (1967). (f) Suenram & Harmony (1973). (g) Spek (1979). (h) Szeimies-Seebach, Harnisch, Szeimies, Van Meerssche, Germain & Declercq (1978). (i) Kobayashi *et al.* (1976). (j) Spek (1977). (k) Hazell (1977). (l) Spek (1978). (m) Declercq, Germain & Van Meerssche (1978). (n) Gougoutas (1979a). (o) Cox, Harmony, Nelson & Wiberg (1969, 1970). (p) Kabuto, Tatsuoka, Murata & Kitahara (1974). (q) Hazell, Pagni & Burnett (1977). (r) Weber & Galantay (1972). (s) Johnson & Schaefer (1972). (t) Gassman & Mullins (1979). (u) Gougoutas (1979b).

recomputed from the atomic coordinates listed in the Cambridge Crystallographic Data File. The tabulated C—C bond lengths vary over a surprisingly wide range. Near one extreme are a substituted tricyclopentane molecule (Gibbons & Trotter, 1967) and the benzene isomer benzvalene (Suenram & Harmony, 1973), both *endo,endo* bridged bicyclobutanes, in which the C(1)—C(3) bond is shorter than the adjacent C—C bonds by 0.095 and 0.077 Å, respectively. Towards

the opposite end of the scale are bicyclobutane-1,3-dicarbonitrile (Johnson & Schaefer, 1972), where the bridge bond was found 0.019 Å longer than the lateral bonds, and an overcrowded *endo,endo*-dimethoxycarbonyl derivative (Gougoutas, 1979b), with a reported difference of nearly 0.06 Å in the same direction.

Two interesting correlations are apparent from the dimensions in Table 4. The average bond length in each

cyclopropane ring, given by $\langle r \rangle = \frac{1}{3}r_{1-3} + \frac{2}{3}r_{1-2}$, is fairly constant throughout the series, with an average value near 1.503 Å, supporting the principle of fixed total bonding proposed by Suenram & Harmony (1972, 1973). Thus, most of the exceptional variability in the bicyclobutane bond lengths is reflected in the single parameter $\Delta r = r_{1-3} - r_{1-2}$. This quantity, moreover, is strongly correlated with the dihedral angle α between the two cyclopropane ring planes. On the average, an increase of 10° in α is associated with an increase of 0.06 Å in the bond-length difference Δr , although the tabulated data scatter rather widely about this linear correlation (Fig. 3).

Even if we exclude the six molecules in which the dihedral angle is compressed by a one- or two-carbon bridge between the C(2) and C(4) positions of the bicyclobutane nucleus, there remains a range of at least 16° in the values of α listed in Table 4. Especially striking is the set of three molecules DBDA, bicyclobutane itself, and bicyclobutane-1,3-dicarbonitrile, all having H atoms in both *endo* positions and thus apparently similar in steric constraints on the dihedral angle, yet with $\alpha = 112.8, 121.7,$ and 126.4° , respectively. It appears that the bicyclobutane skeleton must be quite easily deformable by intra- or intermolecular forces of unspecified nature. Invoking the principle of structural correlation formulated by Dunitz (1979), we can interpret the observed correlation between α and Δr as an indication that skeletal bending and C—C bond-stretching motions are strongly coupled in a low-energy deformation mode of the bicyclobutane nucleus.

In particular, the simultaneous increase in α and Δr evident in Fig. 3 hints at a readily accessible pathway towards the relatively flattened equiangular shape of

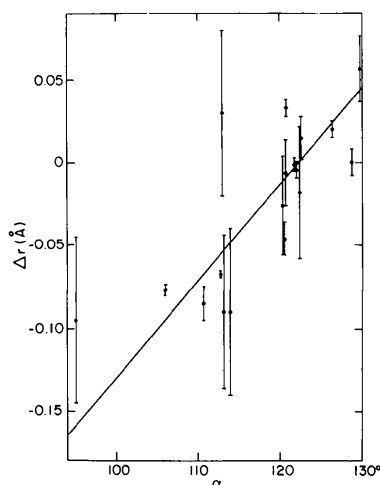


Fig. 3. Bond-length difference Δr vs dihedral angle α in the bicyclobutane derivatives listed in Table 4. Vertical bars indicate the standard deviations given by original authors or estimated from scatter of equivalent bond lengths.

monocyclic cyclobutane, with no bond joining C(1) and C(3). Such a low-energy pathway would account for the thermal *endo-exo* isomerization of substituted 1,3-diphenylbicyclobutanes (Woodward & Dalrymple, 1969), which is thought to proceed *via* a possibly diradical planar transition state (Newton, 1977) or one having only a π -type bonding interaction between C(1) and C(3) (Newton & Schulman, 1972). This interconversion requires the phenyl substituents to pass, at some stage, through the (mean) plane of the C_4 skeleton. Table 4, however, shows no evidence that the opening of the dihedral angle α is accompanied by a widening of the angle $\gamma = C(3)-C(1)-X$ that would bring the bridgehead substituent X nearer to the mean C_4 plane. On the contrary, the tabulated data imply a slightly *negative* correlation between α and γ , in line with the suggestion of Cox *et al.* (1969) and Suenram & Harmony (1973) that the exocyclic C(1)— X bond in bicyclobutane derivatives tends to make equal angles with the C(1)—C(3) and C(1)—C(2) ring bonds. Perhaps the interconversion pathway begins with the flattening of the bicyclobutane nucleus and the stretching of the bridge bond, as suggested by Fig. 3, after which the altered valency at the bridgehead C atoms facilitates the passage of the phenyl substituents to the opposite side of the ring plane.

Deformation density

A comparison of experimental and theoretical charge densities may be performed in different ways. Do we compare static or dynamic deformation densities (Coppens & Stevens, 1977), *i.e.* do we attempt to deconvolute the vibrational motion from our experimental density distribution so as to compare it directly with the theoretical distribution of a stationary molecule or do we smear the theoretical map to simulate the density distribution of a vibrating molecule for comparison with the experimental result? Secondly, do we extract from the periodic density function observed in the crystal a molecular fragment for comparison with theory or do we construct a theoretical crystal density by superposition of symmetrically replicated molecular densities for comparison with the experimental density in the crystal? We have opted in each case for the more crucial test, the one more likely to reveal discrepancies between theory and experiment. Thus, we have elected to compare static rather than dynamic deformation densities. If experiment and theory agree on this level, they must continue to agree after vibrational smearing. If they do not, the disagreement will likely persist in the dynamic densities but in appreciably mitigated form. In the same way we have chosen to compare molecular densities even though this requires a somewhat arbitrary partitioning of the observed crystal density. However, in the

carboxylic acid region, where we expect a significant hydrogen-bonding interaction between neighboring molecules, we have tried to allow for this effect with the aid of theoretical calculations on a similarly hydrogen-bonded dimeric system.

The experimental static deformation density is specified directly, in analytic form, by the refined parameters of our deformation model. Its estimated standard deviation is similarly specified by the least-squares covariance matrix (Rees, 1977). We thus have $\delta\rho$ and $\sigma(\delta\rho)$ at every point in the unit cell, provided the experimental data and the deformation model are both effectively free of systematic bias – but this is one of the main assumptions we hope to test by the comparison with theory. To partition the function $\delta\rho(\mathbf{r})$ into molecular fragments, we have adopted the stockholder recipe for dividing a molecule into atomic fragments (Hirshfeld, 1977b) and applied it to the crystal density in the manner described by Eisenstein (1979). This should introduce no severe uncertainty since, except in the region of the hydrogen-bonded system, neighboring molecules are well separated so that their deformation densities scarcely overlap.

A more serious difficulty is the choice of compounds for the theoretical calculations. The molecule under study is far too large for any reasonable kind of *ab initio* calculation. The only feasible alternative is to compare separate portions of the whole molecule with corresponding model systems small enough to permit such calculations. The model compounds chosen are bicyclobutane, ethane, and formic acid. Such a segmented comparison inevitably links the test of experimental and theoretical deformation densities with the question of transferability between chemically related systems.

The bicyclobutane molecule has been studied by SCF calculations with an extended double- ζ (e.d.z.) basis (Eisenstein & Hirshfeld, 1981). The molecular dimensions (Fig. 4) were taken from the microwave study of Cox *et al.* (1969, 1970) and differ appreciably from those determined here for the substituted derivative. If the difference in bond lengths is real, this must

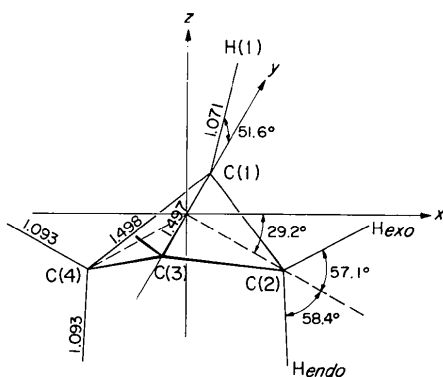


Fig. 4. Bicyclobutane molecular dimensions (\AA and deg) from the microwave study of Cox *et al.* (1969, 1970).

be accompanied by a corresponding difference in the deformation density, if only to satisfy the Hellmann–Feynman theorem. Figs. 5–8 compare four sections

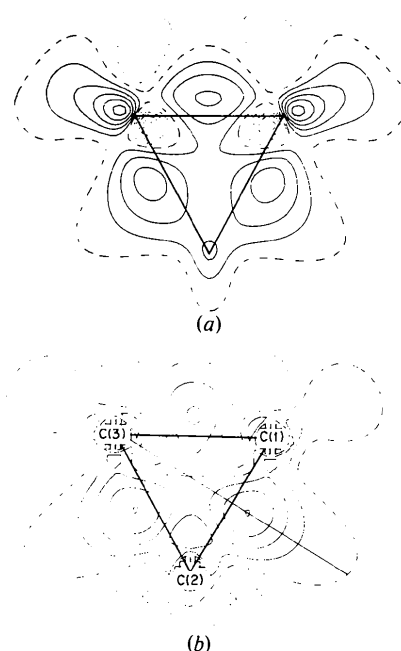


Fig. 5. Deformation density in the C(1)–C(2)–C(3) plane; contour interval 0.1 e \AA^{-3} . (a) DBDA, experimental. (b) Bicyclobutane, theoretical (e.d.z. basis).

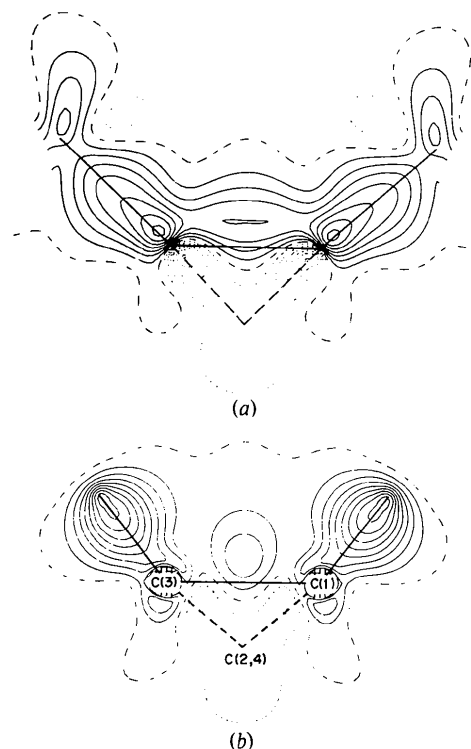
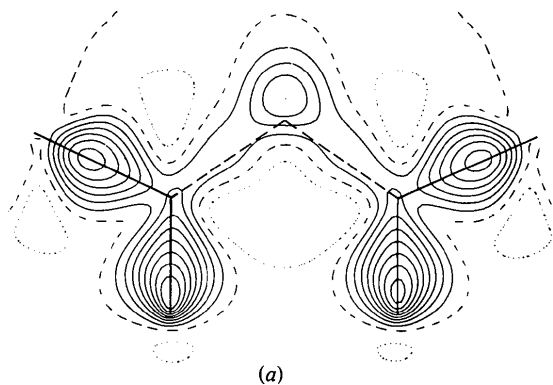
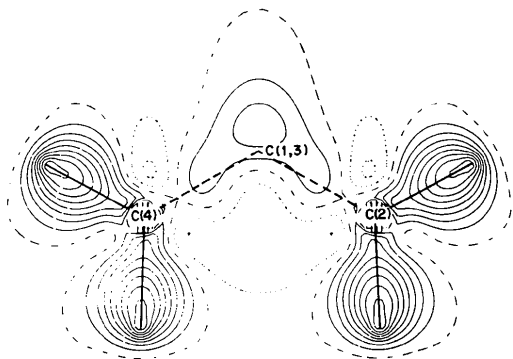


Fig. 6. Deformation density in the yz plane (see Fig. 4 for coordinate system); contour interval 0.1 e \AA^{-3} . (a) DBDA, experimental. (b) Bicyclobutane, theoretical (e.d.z. basis).

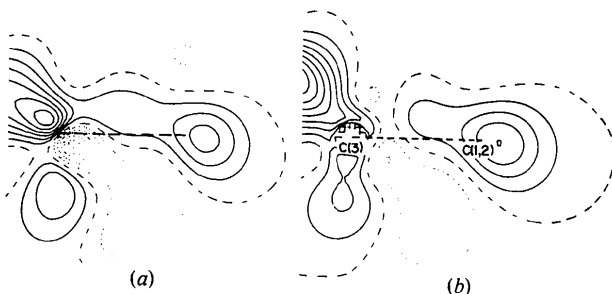


(a)

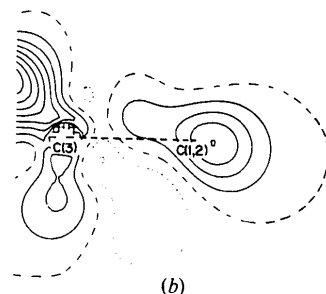


(b)

Fig. 7. Deformation density in the xz plane; contour interval $0.1 \text{ e } \text{\AA}^{-3}$. (a) DBDA, experimental. (b) Bicyclobutane, theoretical (e.d.z. basis).



(a)



(b)

Fig. 8. Deformation density in the section perpendicular to the C(1)—C(2) bond (see trace of section in Fig. 5b); contour interval $0.1 \text{ e } \text{\AA}^{-3}$. (a) DBDA, experimental. (b) Bicyclobutane, theoretical (e.d.z. basis).

through the theoretical deformation density of bicyclobutane with corresponding sections through the present experimental deformation density. Near the heavy-atom centers, no valid comparison is possible. The omission of cusp functions on these atoms has artificially flattened the experimental $\delta\rho$ maps in these regions and has severely depressed the estimated standard deviations $\sigma(\delta\rho)$ listed in Table 5. Had these cusp functions been included, the residual density (see above) implies that they would all have had negative coefficients and so introduced sharp hollows at the atomic centers similar to those seen in the theoretical maps.

Table 5. Experimental deformation density $\delta\rho$ and $\sigma(\delta\rho)$ at atomic centers and bond peaks ($\text{e } \text{\AA}^{-3}$)

Values in the second half-molecule are almost identical to these.

Bond*	$\delta\rho$	$\sigma(\delta\rho)$	Atom	$\delta\rho$	$\sigma(\delta\rho)$
C(1)—C(2)	0.350	0.027	C(1)	0.077	0.041
C(1)—C(3)	0.402	0.029	C(2)	0.228	0.073
C(2)—C(7)	0.648	0.038	C(5)	0.272	0.078
C(5)—C(6)	0.493	0.031	C(6)	0.401	0.120
C(7)—O(1)	0.809	0.079	C(7)	0.123	0.062
C(7)—O(2)	0.512	0.032	O(1)	-0.006	0.081
			O(2)	0.554	0.159
			H(2)	0.932	0.286
			H(5a,b)	0.820	0.199
			H(6a-c)	0.813	0.200
			H(O2)	0.469	0.211

* Bond C(1)—C(5) is omitted because the bond peak is not resolved from the atomic dipole on C(1).

The severe bending of the ring bonds reveals itself in both experimental and theoretical maps by a very similar outward displacement of the C—C bond peaks (Fig. 5). The only appreciable disagreement is in the bridge bond C(1)—C(3), where the experimental map shows a higher peak density [$0.40(3)$ vs $0.27 \text{ e } \text{\AA}^{-3}$] and a much more elongated peak than the theoretical map (Fig. 6). This is the sort of difference that might well account for the pronounced shortening of this bond in the present derivative. But the highly unusual near-in dipolar deformation observed at the bridge-head positions (Fig. 6a) makes us skeptical about the reliability of the experimental deformation density in this region.

In other parts of the bicyclobutane nucleus experiment and theory are in much closer accord. The peak density in the lateral bonds, e.g. C(1)—C(2), shows similar height, shape and position in the two maps (Figs. 5, 8). Even the very slight displacement of this peak out of the cyclopropane-ring plane is nearly identical (0.03 vs 0.02 \AA) in the experimental and theoretical maps (Fig. 8). Furthermore, the small difference in peak density [$0.35(3)$ observed vs $0.40 \text{ e } \text{\AA}^{-3}$ calculated] is again concordant with the difference in bond length (1.519 vs 1.498 \AA).

A more quantitative comparison of the two deformation densities is provided by the moments of the atomic fragments obtained by an atomic partitioning of the molecular charge distributions. Table 6 lists the first few multipole moments, in a local Cartesian system, of the atomic deformation densities defined by the stockholder recipe (Hirshfeld, 1977b) for the atoms C(1), C(2), and H(2) of DBDA and the corresponding atoms of bicyclobutane. Values listed for DBDA are actually averages for corresponding atoms related by the molecular approximate twofold symmetry axis. The net atomic charges in both molecules are all smaller than $\pm 0.1 \text{ e}$ and experimental and theoretical values for corresponding atoms agree in sign. The atomic dipoles

are also small and the agreement in direction is reasonable in view of the difference in substituents on both C atoms. The H atomic dipole in each case is close to the C—H bond direction. The positive second moments μ_{ii} show all atoms to be contracted relative to the free atoms and the anisotropy of the contraction is generally similar in the two molecules. The C charge clouds are somewhat more contracted in DBDA, especially in the direction normal to the local mirror plane, *i.e.* along x for C(1) and along y for C(2). It is impossible to estimate how much of these minor differences is due to inaccuracies in the two deformation densities and how much to genuine differences between the two molecules. The fact that the agreement is generally better for the H than for the C atoms may support the supposition that some of the difference is real and due to chemical substitution.

The experimental deformation density in the C—C—C plane of the ethyl substituent is compared in Fig. 9 with the calculated deformation density of ethane. This calculation was performed with a double- ζ (d.z.) basis only; we therefore expect no more than qualitative agreement. The major differences between the two maps are indeed of the sort that are readily attributable to the absence of polarization functions in the double- ζ basis (Eisenstein, 1979; Stevens, 1980; Eisenstein & Hirshfeld, 1981). Thus, the theoretical bond peaks are appreciably lower and the hollows opposite the bond directions shallower than in the experimental map.

The quantitative comparison (Table 7) is presented in a local axial system on each atom. Moments of the four methylene H atoms in DBDA (5a, 5b, 8a, and 8b) have been averaged, as have those of the six methyl H atoms (6a, 6b, 6c, 9a, 9b, and 9c). In both molecules the C atoms are negatively charged, the H atoms positive, but the charge transfer from H to C is about twice as great in DBDA as in ethane (in the double- ζ approximation). The CH₂ and CH₃ groups are con-

Table 6. Atomic moments in the bicyclobutane nucleus of DBDA compared with corresponding *ab initio* values in bicyclobutane

Units are $10^{-3} e$, $10^{-3} e \text{ \AA}$ and $10^{-3} e \text{ \AA}^2$. See Fig. 4 for local coordinate system.

	C(1)		C(2)		H(2)	
	DBDA	BCB	DBDA	BCB	DBDA	BCB
q	-5	-63	-49	-46	73	25
μ_x	0	0	17	32	-13	3
μ_y	25	22	-3	0	-3	0
μ_z	8	26	10	-2	-89	-75
μ_{xx}	116	85	81	84	67	69
μ_{yy}	49	56	130	96	67	63
μ_{zz}	109	87	107	110	59	58
μ_{xy}	1	0	0	0	-1	0
μ_{yz}	-44	-8	-1	0	1	0
μ_{xz}	0	0	19	13	9	4

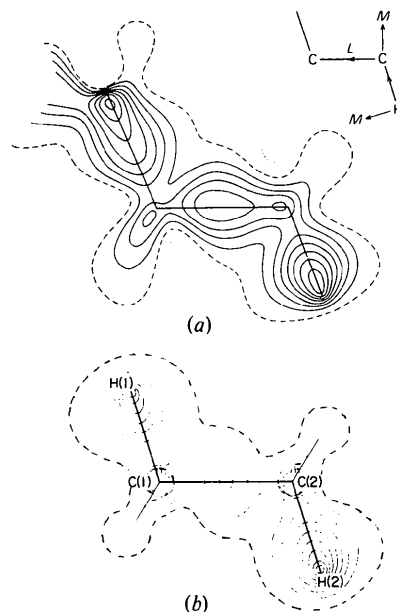


Fig. 9. Deformation density in the ethyl group; contour interval $0.1 e \text{ \AA}^{-3}$. (a) DBDA, C(1)—C(5)—C(6) plane. (b) Ethane H—C—C—H plane (d.z. basis).

Table 7. Average atomic moments in the ethyl groups of DBDA compared with *ab initio* (double- ζ basis) values in ethane

See Fig. 9 for local atomic coordinate systems. Units are $10^{-3} e$, $10^{-3} e \text{ \AA}$ and $10^{-3} e \text{ \AA}^2$.

	C(5)	C(6)	C(ethane)	H(5)	H(6)	H(ethane)
q	-117	-165	-71	57	59	24
μ_L	-14	-11	-15	-81	-86	-68
μ_M	3	2	0	6	2	9
μ_N	14	-12	0	2	-3	0
μ_{LL}	96	88	100	57	63	57
μ_{MM}	138	145	132	56	66	71
μ_{NN}	80	118	132	78	74	73
μ_{LM}	6	6	0	4	2	-3
μ_{MN}	-5	1	0	-2	-1	0
μ_{LN}	-7	-7	0	2	2	0

sistently neutral although only in ethane is this demanded by molecular symmetry. In both molecules the C atoms are very slightly polarized into the ethyl C—C bond, while the H atoms are strongly polarized along the C—H axes. All atoms have positive diagonal second moments and the charge contraction this implies is nearly isotropic but tends to be somewhat smaller than average along the C—C bond for C and along the C—H bond for H. The overall agreement is about as satisfactory here as in the bicyclobutane nucleus despite the poorer quality of the ethane wavefunction. This apparent success of the double- ζ basis may be related to the apolarity of the ethane molecule.

For comparison with the experimental deformation density in the carboxylic region of the molecule, four theoretical calculations have been performed on the formic acid system. One is an extended-basis calculation on formic acid itself. The other three are double- ζ calculations on formic acid, in two geometries, and on its cyclic hydrogen-bonded dimer. The two monomer geometries (Fig. 10) are those reported (Almenningen, Bastiansen & Motzfeldt, 1969) for the isolated monomer and for the gas-phase dimer. The dimer calculation was performed at the observed dimer geometry, adjusted to an O...O distance equal to that found in the DBDA crystal. (The crystal contains two non-equivalent hydrogen bonds, with O...O distances of 2.59 and 2.65 Å; the latter distance was adopted for the formic acid calculation.)

These calculations enable us to trace the changes in the deformation density of formic acid on formation of the hydrogen-bonded dimer. The overall process can be divided conceptually into three stages: a geometric modification of the individual monomer molecules, juxtaposition of these monomers in the dimer configuration, and charge migration in the dimer. The first stage

is evidently of minor consequence; the change in monomer dimensions is not well established experimentally and, in any case, the calculated effect on the deformation density is quite small. The effect of juxtaposition is appreciable mainly in the immediate vicinity of the hydrogen bond. Here the charge deficiency behind the hydroxyl H atom overlaps and partly cancels the excess lone-pair density of the acceptor O atom. The most conspicuous effect on the deformation density map is an inward displacement of the zero contour around the acceptor lobe of the carbonyl O (Fig. 10*c,d*). The mutual cancellation of positive and negative densities produces a formal transfer of 0.09 e from O(1) to H(2) (Table 8).

The actual charge migration in the hydrogen-bonded dimer is seen in Fig. 11, which plots the difference, in the double- ζ approximation, between the deformation densities of the dimer and of the two juxtaposed monomer molecules. This charge redistribution may, as in the systems studied by Yamabe & Morokuma (1975), be attributed primarily to two effects: an exchange interaction, which removes charge from the intermolecular overlap region in accordance with the

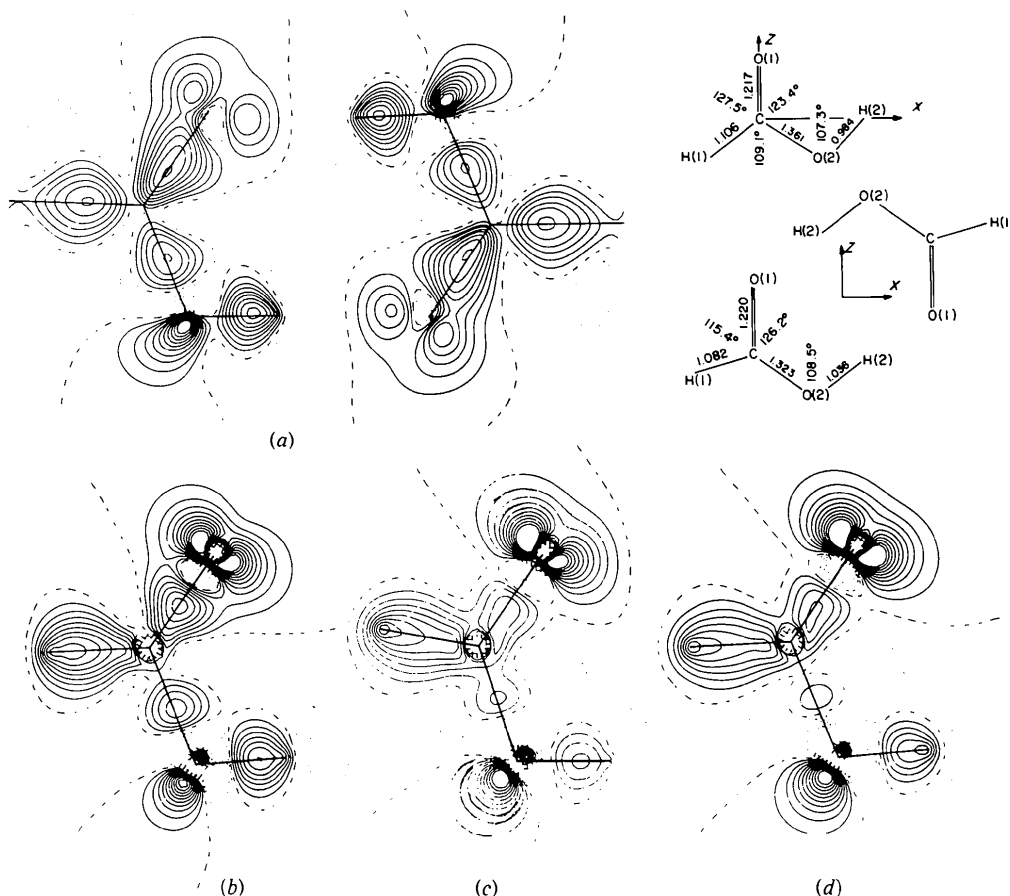


Fig. 10. Experimental deformation density in carboxylic acid cyclic dimer compared with the *ab initio* deformation density of formic acid; contour interval $0.1 \text{ e } \text{Å}^{-3}$. (a) DBDA, mean plane of carboxylic acid dimer. (b) Formic acid monomer, e.d.z. basis. (c) Formic acid dimer, d.z. basis. (d) Formic acid monomer, d.z. basis.

Table 8. Atomic moments in DBDA compared with *ab initio* moments in formic acid monomer (*M*), juxtaposed monomers in dimer geometry ($2M'$), and dimer (*D*)

' $D_{e.d.z.}$ ' represents the synthetic combination $M_{e.d.z.} + D_{d.z.} - M_{d.z.}$. Units are $10^{-3} e$, $10^{-3} e \text{ \AA}$ and $10^{-3} e \text{ \AA}^2$. See Fig. 10 for local coordinate system.

	$M_{e.d.z.}$	$M_{d.z.}$	$2M'_{d.z.}$	$D_{d.z.}$	' $D_{e.d.z.}$ '	DBDA
O(1) q	-330	-331	-243	-300	-299	-221
μ_x	4	10	70	80	74	24
μ_z	-62	-167	-113	-122	-17	-2
μ_{xx}	-77	-90	-32	-34	-21	30
μ_{yy}	-35	-40	-8	-27	-22	38
μ_{zz}	-34	-36	11	9	11	2
μ_{xz}	-1	-2	27	33	34	13
C q	272	280	275	295	287	184
μ_x	8	27	35	28	9	22
μ_z	-57	-29	-27	-20	-48	-31
μ_{xx}	137	154	150	157	140	104
μ_{yy}	279	261	264	283	301	244
μ_{zz}	52	65	84	80	67	75
μ_{xz}	20	25	35	39	34	-5
O(2) q	-219	-234	-226	-235	-220	-139
μ_x	-3	-17	-22	-7	7	35
μ_z	81	190	183	187	78	65
μ_{xx}	74	79	68	72	67	80
μ_{yy}	-19	-41	-38	-35	-13	65
μ_{zz}	-6	-27	-31	-32	-11	12
μ_{xz}	14	17	5	1	-2	4
H(2) q	198	198	111	154	154	149
μ_x	102	92	22	25	35	31
μ_z	64	61	12	15	18	9
μ_{xx}	100	103	33	34	31	36
μ_{yy}	93	93	56	64	64	90
μ_{zz}	79	73	41	48	54	59
μ_{xz}	1	-2	-31	-34	-31	-26

demands of the Pauli exclusion principle, and a mutual electrostatic polarization of the monomer charge distributions. Both these effects act in concert to enhance the polarization of the O—H bond, removing charge from H and transferring it to a region that corresponds essentially to a p_σ orbital on the hydroxyl O atom O(2). A similar but greatly attenuated pattern of σ -bond polarization carries further a small fraction of the displaced charge from O(2) to the C atom and from C to the carbonyl O atom O(1) (Fig. 11). At the acceptor O the exchange effect appears to predominate over the electrostatic polarization, causing a net removal of charge from the forward lone-pair lobe. This charge is displaced to the far side of O(1), causing a highly diffuse broadening of the distant lone-pair lobe. The net charge on O(1) increases by 0.06 e relative to the juxtaposed monomers (Table 8), much of this increase being attributable to a polarization of the π density in the carbonyl bond, as revealed by a more negative μ_{yy} on O(1) and a correspondingly more positive μ_{yy} on C. A very similar pattern was described by Flood (1974), whose Mulliken population analysis showed O(1) to gain π charge on dimerization at the

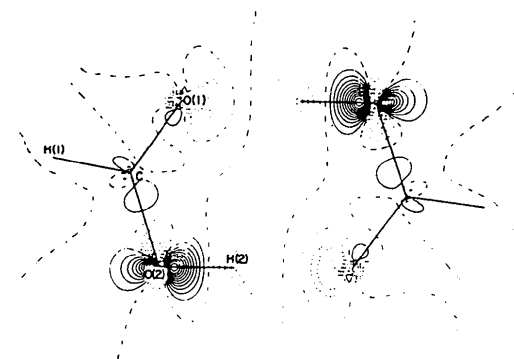


Fig. 11. Formic acid difference density: dimer minus juxtaposed monomers, d.z. basis; contour interval $0.025 e \text{ \AA}^{-3}$.

expense of C and O(2), while the loss at O(2) was more than compensated by a parallel increase in the σ charge on this atom.

For comparison with the experimental deformation density in DBDA, we can approximate the deformation density in the formic acid dimer as

$$\delta\rho(\text{dimer}) \sim \delta\rho_{e.d.z.}(\text{monomer}_2) + \delta\rho_{d.z.}(\text{dimer}) - \delta\rho_{d.z.}(\text{monomer}_2), \quad (2)$$

in which the extended-basis result for the monomer is adjusted by the difference, in the double- ζ approximation, between the monomer and dimer deformation densities. This synthetic deformation density suffers from a slight ambiguity in definition because of the small difference in molecular geometry between the monomer and the dimer. But in practice this is not a severe obstacle to local comparisons of experimental and theoretical maps. For example, in the O(1)=C—O(2) region of formic acid, the second molecule makes a completely negligible contribution, so that $\delta\rho(\text{monomer}_2) \sim \delta\rho(\text{monomer})$, while the difference between monomer and dimer is also small, *i.e.* $\delta\rho(\text{dimer}) - \delta\rho(\text{monomer}_2) \sim 0$. Thus we can, in this region, compare the experimental deformation density in DBDA (Fig. 10a) directly with the e.d.z. map of formic acid monomer (Fig. 10b). The experimental peak density in the C=O(1) bond is $0.81(8)$ vs $0.75 e \text{ \AA}^{-3}$ theoretical, while the corresponding comparison for the C—O(2) bond shows $0.51(3)$ vs $0.46 e \text{ \AA}^{-3}$. Qualitative features are also similar in the two maps, such as the positions and shapes of lone-pair peaks on both O atoms and the disposition of negative hollows around the C atom and near the O ends of the two C—O bonds. Appreciable differences are found mainly in the region of the hydrogen bond, where the effect of dimerization is greater. Thus, the zero contour turns back around the acceptor lobe of O(1) in DBDA (Fig. 10a) just as in the formic acid dimer (Fig. 10c).

Table 8, which lists the atomic moments for the acid portion of DBDA together with corresponding quantities from the several formic acid calculations, also gives the synthetic 'e.d.z. dimer' values for formic acid,

evaluated according to the recipe implied in eq. (2). These are the quantities most appropriate for comparison with the experimental values for DBDA. For atoms O(1) and H(2), which are directly involved in the hydrogen bond, the synthetic 'e.d.z. dimer' moments agree much better than the monomer values with the experimental moments. Thus, the charge on O(1) is reduced from -0.33 in the formic acid monomer to -0.30 e in the dimer, somewhat closer to the DBDA value of -0.22 e, while its dipole moment, which points close to the $-z$ direction in the monomer, adopts a transverse orientation in the dimer as in DBDA, though with a magnitude three times as great. The positive charge on H decreases (*via* juxtaposition) from 0.20 to 0.15 e on dimerization, in agreement with the value in DBDA, while its dipole moment drops from 0.12 to 0.04 e Å, compared to 0.03 e Å in DBDA. The hydroxyl O atom O(2), far less influenced by dimerization, shows only moderate agreement with the DBDA results. The C atom, which becomes slightly more positive in the dimer, is not properly comparable because of its different chemical surroundings in the two molecules. Both C—O bonds are far less polar in DBDA than in formic acid (monomer or dimer) and much of the disparity is concentrated in the π density, as indicated by substantial differences in the μ_{yy} second moments between 'D_{e.d.z.}' and DBDA. On all three atoms in the O=C—O chain these differences have the same sign as the differences in atomic charge q .

In her study of diformohydrazone, Eisenstein (1979) performed a similar comparison between experimental and theoretical multipole moments of the partitioned atomic deformation densities. The result was a marginally better agreement in atomic charges than that found here, probably because the X-ray data used were more accurate, but a progressively poorer match in the dipole and second moments. The discrepancies in that case are partly attributable to the influence of the intermolecular hydrogen bond in the diformohydrazone crystal, which was neglected in the comparison with the e.d.z. deformation density of formamide. The disagreement in second moments had a clearly systematic component, with the experimental values consistently more positive than the theoretical. In both studies the agreement seems to be slightly better for H than for the heavier atoms. The scanty evidence presently available does not yet warrant a detailed interpretation of such apparent regularities.

We are grateful to Dr Ziva Berkovitch-Yellin, of this Department, for valued computational assistance. This research was supported by a grant from the United States—Israel Binational Science Foundation (BSF), Jerusalem, Israel.

Addendum: The positive correlation between the bridge bond length r_{1-3} and the dihedral angle α in

bicyclobutane derivatives (Table 4 and Fig. 3) has been noted previously by Irngartinger & Lukas (1979). A theoretical argument proposed by Paddon-Row, Houk, Dowd, Garner & Schappert (1981), supported by *ab initio* calculations on bicyclobutane with the angle α fixed at different values between 90 and 130° , qualitatively accounts for the observed increase in r_{1-3} as well as the concomitant decrease in r_{1-2} and in the bridgehead angle γ with increasing α . We are grateful to Professor Jack Dunitz for bringing these references to our attention.

References

- ALMENNINGEN, A., BASTIANSEN, O. & MOTZFELDT, T. (1969). *Acta Chem. Scand.* **23**, 2848–2864.
- BUSING, W. R. & LEVY, H. A. (1964). *Acta Cryst.* **17**, 142–146.
- COPPENS, P. (1968). *Acta Cryst.* **A24**, 253–257.
- COPPENS, P. & STEVENS, E. D. (1977). *Isr. J. Chem.* **16**, 175–179.
- COX, K. W., HARMONY, M. D., NELSON, G. & WIBERG, K. B. (1969). *J. Chem. Phys.* **50**, 1976–1980.
- COX, K. W., HARMONY, M. D., NELSON, G. & WIBERG, K. B. (1970). *J. Chem. Phys.* **53**, 858.
- DECLERCQ, J. P., GERMAIN, G. & VAN MEERSSCHE, M. (1978). *Acta Cryst.* **B34**, 3472–3474.
- DENNE, W. A. (1977). *Acta Cryst.* **A33**, 438–440.
- DUNITZ, J. D. (1979). *X-ray Analysis and the Structure of Organic Molecules*, p. 363. Ithaca: Cornell Univ. Press.
- EISENSTEIN, M. (1979). *Acta Cryst.* **B35**, 2614–2625.
- EISENSTEIN, M. & HIRSHFELD, F. L. (1981). *Chem. Phys.* **54**, 159–172.
- FLOOD, E. (1974). *J. Mol. Struct.* **21**, 221–229.
- GASSMAN, P. G. & MULLINS, M. J. (1979). *Tetrahedron Lett.* pp. 4457–4460.
- GERMAIN, G., MAIN, P. & WOOLFSON, M. M. (1971). *Acta Cryst.* **A27**, 368–376.
- GIBBONS, C. S. & TROTTER, J. (1967). *J. Chem. Soc. A*, pp. 2027–2031.
- GOUGOUTAS, J. Z. (1979a). *Cryst. Struct. Commun.* **8**, 131–134.
- GOUGOUTAS, J. Z. (1979b). *Cryst. Struct. Commun.* **8**, 135–138.
- HAREL, M. & HIRSHFELD, F. L. (1975). *Acta Cryst.* **B31**, 162–172.
- HAZELL, A. C. (1977). *Acta Cryst.* **B33**, 272–274.
- HAZELL, A. C., PAGNI, R. M. & BURNETT, M. (1977). *Acta Cryst.* **B33**, 2344–2346.
- HIRSHFELD, F. L. (1976). *Acta Cryst.* **A32**, 239–244.
- HIRSHFELD, F. L. (1977a). *Isr. J. Chem.* **16**, 226–229.
- HIRSHFELD, F. L. (1977b). *Theor. Chim. Acta*, **44**, 129–138.
- HOPE, H. & OTTERSEN, T. (1978). *Acta Cryst.* **B34**, 3623–3626.
- IRNGARTINGER, H. & LUKAS, K. L. (1979). *Angew. Chem. Int. Ed. Engl.* **18**, 694–695.
- JOHNSON, C. K. (1970). *Thermal Neutron Diffraction*, edited by B. T. M. WILLIS, pp. 132–160. Oxford Univ. Press.
- JOHNSON, P. L. & SCHAEFER, J. P. (1972). *J. Org. Chem.* **37**, 2762–2763.
- KABUTO, C., TATSUOKA, T., MURATA, I. & KITAHARA, Y. (1974). *Angew. Chem. Int. Ed. Engl.* **13**, 669–670.
- KOBAYASHI, Y., KUMADAKI, I., OHSAWA, A., HANZAWA, Y., HONDA, M., IITAKA, Y. & DATE, T. (1976). *Tetrahedron Lett.* pp. 2545–2548.
- MARGOTTIN-MACLOU, M. (1960). *J. Phys. Radium*, **21**, 634–644.
- MEIBOOM, S. & SNYDER, L. C. (1971). *Acc. Chem. Res.* **4**, 81–87.
- NEWTON, M. D. (1977). *Methods of Electronic Structure Theory*, edited by H. F. SCHAEFER, pp. 223–275. New York: Plenum.

- NEWTON, M. D. & SCHULMAN, J. M. (1972). *J. Am. Chem. Soc.* **94**, 767–773.
- PADDON-ROW, M. N., HOUK, K. N., DOWD, P., GARNER, P. & SCHAPPERT, R. (1981). *Tetrahedron Lett.* **22**, 4799–4802.
- REES, B. (1977). *Isr. J. Chem.* **16**, 180–186.
- SPEK, A. L. (1977). *Cryst. Struct. Commun.* **6**, 259–262.
- SPEK, A. L. (1978). *Cryst. Struct. Commun.* **7**, 303–308.
- SPEK, A. L. (1979). *Cryst. Struct. Commun.* **8**, 325–330.
- STEVENS, E. D. (1980). *Acta Cryst.* **B36**, 1876–1886.
- SUENRAM, R. D. & HARMONY, M. D. (1972). *J. Chem. Phys.* **56**, 3837–3842.
- SUENRAM, R. D. & HARMONY, M. D. (1973). *J. Am. Chem. Soc.* **95**, 4506–4511.
- SZEIMIES-SEEBACH, U., HARNISCH, J., SZEIMIES, G., VAN MEERSSCHE, M., GERMAIN, G. & DECLERCQ, J. P. (1978). *Angew. Chem. Int. Ed. Engl.* **17**, 848–850.
- WEBER, H. P. & GALANTAY, E. (1972). *Helv. Chim. Acta*, **55**, 544–553.
- WOODWARD, R. B. & DALRYMPLE, D. L. (1969). *J. Am. Chem. Soc.* **91**, 4612–4613.
- YAMABE, S. & MOROKUMA, K. (1975). *J. Am. Chem. Soc.* **97**, 4458–4465.

Acta Cryst. (1983). **B39**, 75–84

Structural Phase Transition in Polyphenyls.

VIII. The Modulated Structure of Phase III of Biphenyl ($T \simeq 20$ K) from Neutron Diffraction Data

BY J. L. BAUDOUR AND M. SANQUER

Groupe de Physique Cristalline, ERA au CNRS n° 07015, Université de Rennes, Campus de Beaulieu, 35042 Rennes CEDEX, France

(Received 15 March 1982; accepted 14 June 1982)

Abstract

Starting from the approximation of the superstructure [Cailleau, Baudour & Zeyen (1979). *Acta Cryst.* **B35**, 426–432] the modulated structure of deuterated biphenyl (phase III, $T \simeq 20$ K) has been determined by taking into account 265 main reflections and 273 first-order satellites. The de Wolff–Janssen–Janner (3 + 1)-dimensional superspace group is the non-centrosymmetric $P\bar{1}^a$, although the symmetry of the centrosymmetric group $P\bar{1}^{P2_1/a}$ is almost respected. The refinement based on a harmonic displacive modulation has been performed with a very limited number of variable parameters: four positional parameters, phenyl rings being described by rigid blocks, 11 thermal parameters (individual isotropic Debye–Waller factors), and six modulation parameters: three amplitudes and three phases. The final value of R is 0.106 (0.088 for main reflections, 0.176 for satellites). The main features of the modulation are (a) a torsion around the long molecular axis with a maximum deformation of 11° , (b) a rotation around the normal to the mean molecular plane with an amplitude of 1.0° , 90° out of phase with the torsion, and (c) a translation along the long molecular axis with an amplitude of 0.035 \AA , in phase with the torsion.

Introduction

At about 40 K biphenyl undergoes a structural phase transition induced by a so-called soft phonon observed

with Raman spectroscopy (Bree & Edelson, 1977). In a first neutron diffraction study (Cailleau, Baudour & Zeyen, 1979) this structural phase transition had been interpreted as resulting from the appearance of superlattice reflections at the $B(0, \frac{1}{2}, 0)$ point of reciprocal space, corresponding to a doubling of the b parameter only and not to the doubling of a and b as found for other polyphenyls: p -terphenyl (Baudour, Delugeard & Cailleau, 1976) and p -quaterphenyl (Baudour, Delugeard & Rivet, 1978).

The space group of biphenyl at room temperature is $P2_1/a$ with two planar molecules on inversion sites (Hargreaves & Rizvi, 1962; Trotter, 1961; Robertson, 1961) and the essential structural modifications in the low-temperature phase result, as in other polyphenyls, from a torsion angle between the planes of phenyl groups. In biphenyl this angle was estimated from the first study (Cailleau, Baudour & Zeyen, 1979) to be about 10° and was in opposite senses for two neighbouring molecules along b .

More recent elastic neutron scattering measurements (Cailleau, Moussa & Mons, 1979) performed on a cold-source triple-axis spectrometer (with $\lambda = 4.1 \text{ \AA}$ instead of $\lambda = 1.26 \text{ \AA}$ in the first study) gave a higher resolution and showed clearly that each 'pseudo superlattice reflection' could be resolved into four or two (this number depending upon the temperature) satellite reflections typical for a modulated structure (Fig. 1). So, in fact, the new reflections appearing at low temperature were not characterized by the commensurate wavevector $\mathbf{q}^* =$